RESEARCH PAPER

Channels 6:4, 317-331; July/August 2012; © 2012 Landes Bioscience

The gating mechanism of the bacterial mechanosensitive channel MscL revealed by molecular dynamics simulations

From tension sensing to channel opening

Yasuyuki Sawada,[1] Masaki Murase[2] and Masahiro Sokabe[1-3,*]

[1]Department of Physiology; Nagoya University Graduate School of Medicine; Showa-ku, Nagoya, Japan; [2]International Cooperative Research Project/Solution Oriented Research for Science and Technology Cell Mechanosensing; Japan Science and Technology Agency; Showa-ku, Nagoya, Japan; [3]First Research Center for Innovative Nanobiodevice; Nagoya University; Nagoya, Japan

Keywords: mechanosensitive channel, MscL, tension sensing, gating, molecular dynamics simulation, MscL mutants

One of the ultimate goals of the study on mechanosensitive (MS) channels is to understand the biophysical mechanisms of how the MS channel protein senses forces and how the sensed force induces channel gating. The bacterial MS channel MscL is an ideal subject to reach this goal owing to its resolved 3D protein structure in the closed state on the atomic scale and large amounts of electrophysiological data on its gating kinetics. However, the structural basis of the dynamic process from the closed to open states in MscL is not fully understood. In this study, we performed molecular dynamics (MD) simulations on the initial process of MscL opening in response to a tension increase in the lipid bilayer. To identify the tension-sensing site(s) in the channel protein, we calculated interaction energy between membrane lipids and candidate amino acids (AAs) facing the lipids. We found that Phe78 has a conspicuous interaction with the lipids, suggesting that Phe78 is the primary tension sensor of MscL. Increased membrane tension by membrane stretch dragged radially the inner (TM1) and outer (TM2) helices of MscL at Phe78, and the force was transmitted to the pentagon-shaped gate that is formed by the crossing of the neighboring TM1 helices in the inner leaflet of the bilayer. The radial dragging force induced radial sliding of the crossing portions, leading to a gate expansion. Calculated energy for this expansion is comparable to an experimentally estimated energy difference between the closed and the first subconductance state, suggesting that our model simulates the initial step toward the full opening of MscL. The model also successfully mimicked the behaviors of a gain of function mutant (G22N) and a loss of function mutant (F78N), strongly supporting that our MD model did simulate some essential biophysical aspects of the mechano-gating in MscL.

Introduction

Mechanosensation is an essential process by which cells respond to changes in mechanical stress in the cell. In fact, mechanosensitive (MS) channels play important roles not only in hearing, touch and cardiovascular regulation, but also in regulating the volume, morphology and migration of cells.[1] In bacteria, MS channels are critical to maintain the viability of the cell against hypo-osmotic pressures.[2,3]

One of the bacterial MS channels, mechanosensitive channel of large conductance (MscL), is the first MS channel for which the gene and 3D protein structure were determined.[4,5] Purified MscL reconstituted into the lipid bilayer was found to retain its native mechanosensitive function, indicating that MscL activation is brought about exclusively by stress in the membrane and does not require any supporting proteins.[6,7] Patch-clamp experiments showed that MS channels are activated by tension in the membrane rather than by either transmural pressure across the membrane or membrane curvature.[6-9]

Ion channels in general, including MS channels, have two conducting states called open and closed, respectively. Detailed analyses of the conductance levels and the kinetics of state transitions in MscL have revealed that at least five subconductance states exist on the way to the fully open state.[6] It was estimated that the first conductance state is the rate-limiting step, with a free energy level higher than that of the closed state by approximately 38 k_BT and with an averaged pore radius of approximately 4.0 Å.[6]

The MS channels for which the crystal structure has been obtained are MscL and mechanosensitive channel of small conductance(MscS). MscL was first characterized in *Escherichia coli*, but the obtained crystal structure is only from *Mycobacterium tuberculosis* and is thus referred to as Tb-MscL, as shown in **Figure 1A and B** (PDB accession number: 1MSL).[5] Tb-MscL has an overall sequence identity of 37% with the MscL from

*Correspondence to: Masahiro Sokabe; Email: msokabe@med.nagoya-u.ac.jp
Submitted: 05/11/12; Revised: 08/13/12; Accepted: 08/20/12
http://dx.doi.org/10.4161/chan.21895

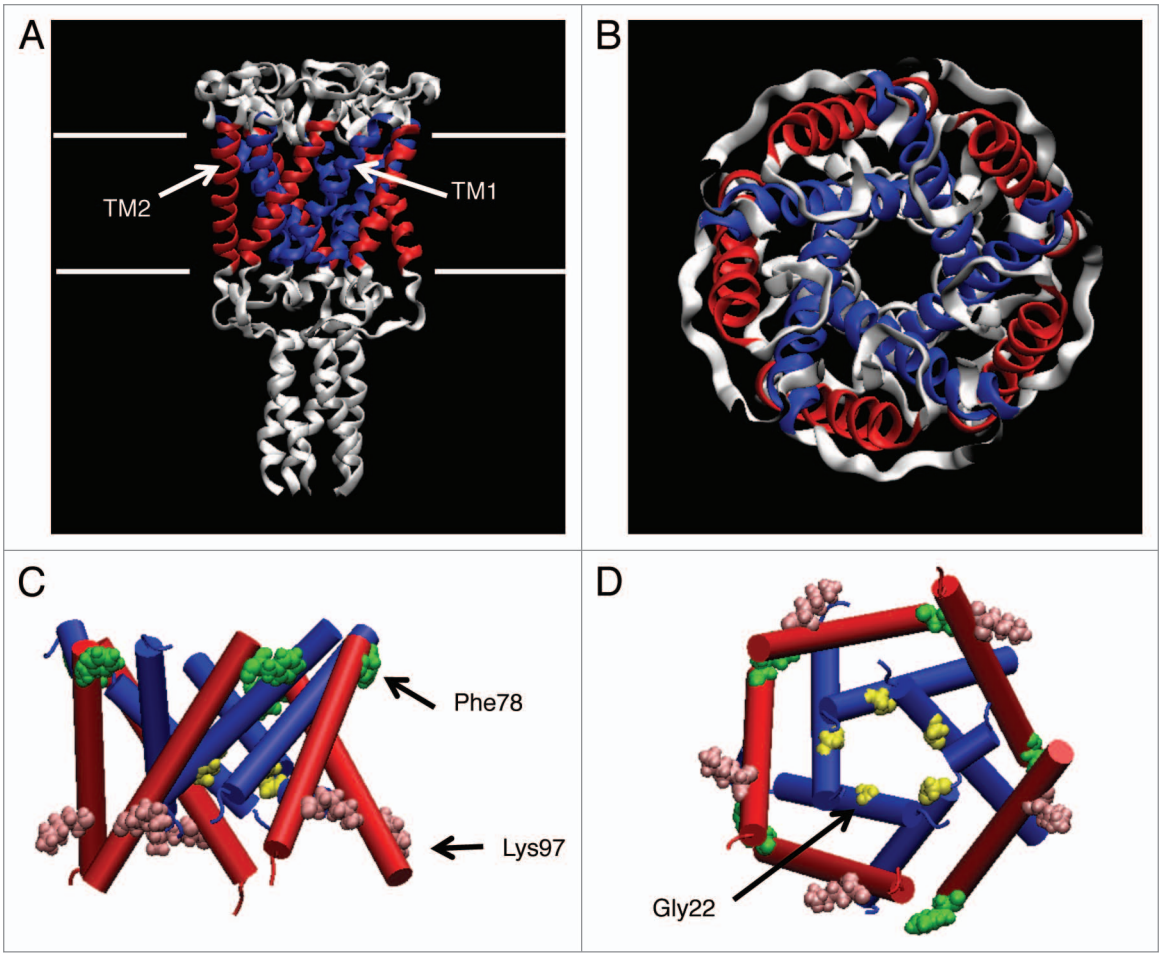

Figure 1. Crystal structure of MscL. The side (**A**) and top (**B**) views of the MscL from *Mycobacterium tuberculosis* (PDB code: 1MSL), where the TM1 and TM2 helices are colored in blue and red, respectively. The side (**C**) and bottom (**D**) views of the 3D structure of Eco-MscL used in our simulations (only the transmembrane helices are shown) with Gly22 (yellow), Phe78 (green) and Lys97 (pink) depicted as a VDW representation.

Escherichia coli (Eco-MscL), with a comparable conductance as Eco-MscL.[10] The structure of Tb-MscL suggests that it is mostly in a closed form, and its open structure has not been resolved yet. As most of the experiments to date have been done with Eco-MscL, a molecular model for Eco-MscL was constructed based on the crystal structure of Tb-MscL to allow structure-function investigation of MscL.[7] Eco-MscL (hereafter this will be denoted simply as MscL unless otherwise noted) forms a homopentamer, with a subunit having two transmembrane helices consisting of 136 amino acids (AAs), and with a molecular weight of 15 kDa.[4,6] The first transmembrane (TM1) helices line the pore and the second transmembrane (TM2) helices form the outer wall facing the lipids surrounding MscL (**Fig. 1**). The sequence toward the N terminus has a helix structure named S1, forming a bundle with the cytoplasmic helix, and also with a sequence toward the C terminus, although the most N-terminal region of the first published structure was not resolved.[5] In a later version of the Tb-MscL crystal structure published in 2007, the S1 helix was better resolved and more precisely modeled (PDB; 2OAR).[11] The S1 in the revised version has a helical structure running parallel to the cytoplasmic membrane surface instead of forming a tight bundle as proposed in the earlier model. In the earlier model, the S1 helices are supposed to associate together to plug the cytoplasmic opening of the pore and form a secondary gate.[12]

Many studies have been performed using site-directed mutagenesis in order to better understand the structure-function of MscL.[13-19] One of these studies produced an estimation of the tension-sensing site in MscL using random scanning mutagenesis, where individual hydrophobic AAs facing the lipids were replaced with the hydrophilic AA asparagine to identify any "loss-of-function" mutants lacking mechanosensitivity.[15] As the result, it was found that replacement of one of seven amino residues located at the periplasmic end of the transmembrane helices caused the loss of MscL mechanosensitivity, suggesting that one or some of them may act as a tension sensor in MscL. On the other hand, when Gly22, located near the most constricted part of the ion permeation pore that is considered to be a compartment of the mechanosensitive gate of MscL, is substituted to another AA, typically asparagine (G22N), the resulting mutants could more easily be opened (gain-of-function) in comparison with the wild-type (WT) MscL.[13,16]

Table 1. Summary of the major parameters (membrane tension and simulation time) and the radii obtained for the most constricted part (gate) of the MscL pore

Type of MscL	Generated surface tension (dyn/cm)	Simulation time (ns)	Pore size (Å)	
			0 ns	2 ns
WT	0	5.0	1.5	1.9
	150	2.0	1.5	5.8
F78N	150	2.0	1.5	3.3
G22N	0	5.0	2.0	3.8

The simulation time does not include the time for system equilibration. WT, wild-type; F78N, a loss-of-function mutant created by the substitution of Phe78 with Asn78; G22N, a gain-of-function mutant created by the substitution of Gly22 with Asn22.

In order to examine the structural changes during the opening of MscL in atomic detail, molecular simulations, including all atom and coarse-grained models, have been conducted.[20-28] The first problem to simulate channel opening is how to apply forces to a modeled MscL. One method employed force tethered to particular AAs or whole-channel proteins.[20,21,24,27] This method could somehow simulate MscL opening behaviors, but with some abnormal structural changes of MscL. Another method is to generate stress in the MscL-embedded membrane by modifying the bilayer structure.[25,26] This method is based on the findings that pressure distribution in the membrane varies with the type of the membrane and that the pressure profile of the membrane affects the channel gating,[22] however, it could not induce MscL opening within the simulation period,[25] or only revealed that how MscL adapt to a thinner membrane.[26] Therefore, it is critically important to develop a stimulation method that can mimic the membrane stretching, which is used in most experiments to stimulate MscL.

To address these problems, we constructed a molecular model using the MscL, lipid bilayer and water, and performed MD simulations on MscL opening under increased membrane tension, which was generated by reducing the lateral pressure only in the bilayer. This method enabled an analysis of the protein-lipid interactions on the surface of the transmembrane helices facing lipids, which are crucial for identifying the tension-sensing site in MscL. Meanwhile, all-atom MD simulations of proteins have limitations, such as a relatively short simulation time. A few 10ths of nanoseconds (ns) is the upper limit for the simulation to produce reliable results. This period is apparently much shorter than the actual opening process of MscL. At least a few hundred microseconds (μs) is required to reach the full open state of MscL.[6] Therefore, we focused on the initial process of MscL opening to resolve two mechanisms critical for further opening, (1) which residue(s) has the most potent interaction with the surrounding lipids (identification of tension sensing site(s) in MscL) and (2) how the received force by the tension-sensing site(s) induces expansion of the most constricted region (gate) of the pore. Finally, to evaluate whether the model and the condition set in the simulation are appropriate for analyzing the MscL opening process, we constructed molecular models for two mutants that are known to open more easily (G22N) or with greater difficulty (F78N) than WT MscL, and examined whether they were able to reproduce the essence of experimentally observed features.[13,15,16]

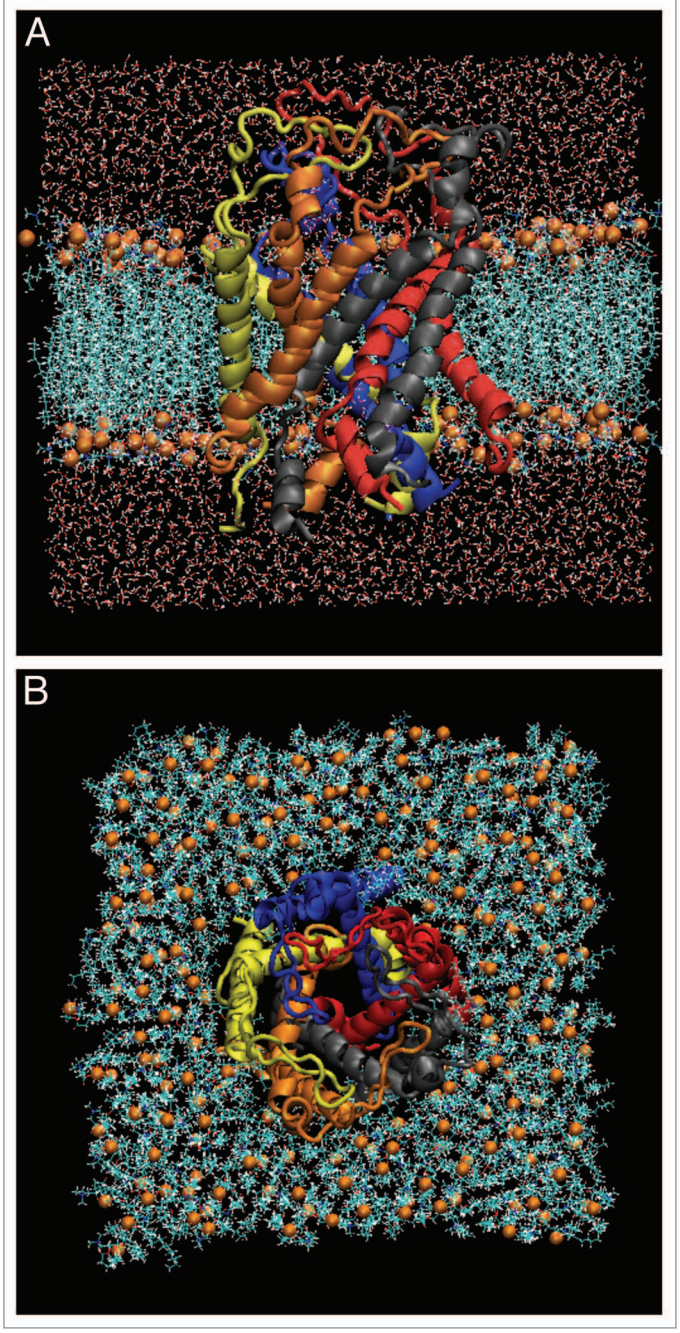

Figure 2. The side (**A**) and top (**B**) views of our simulation model consisting of WT-MscL, POPC and water molecules at 0 ns. The side (**A**) and top (**B**) views. MscL is shown in a ribbon drawing with different colors for each subunit. The water molecules are shown in red (oxygen atoms) and white (hydrogen atoms) colors. The phosphate atoms of individual lipid molecules are shown in orange in the space-filling drawing.

Results

Stability of the MscL structure during equilibration calculation. To analyze the stability of the MscL structure in the lipid

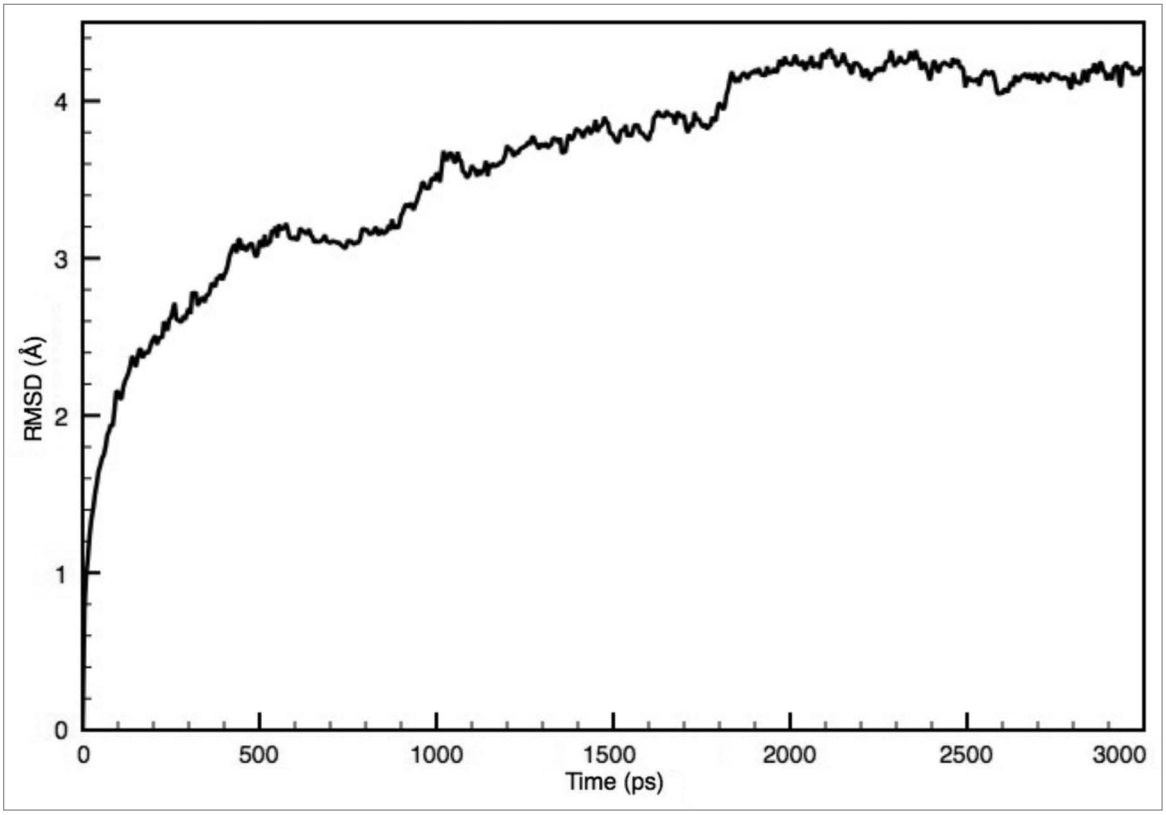

Figure 3. Time-course of RMSD with respect to the initial structure of MscL.

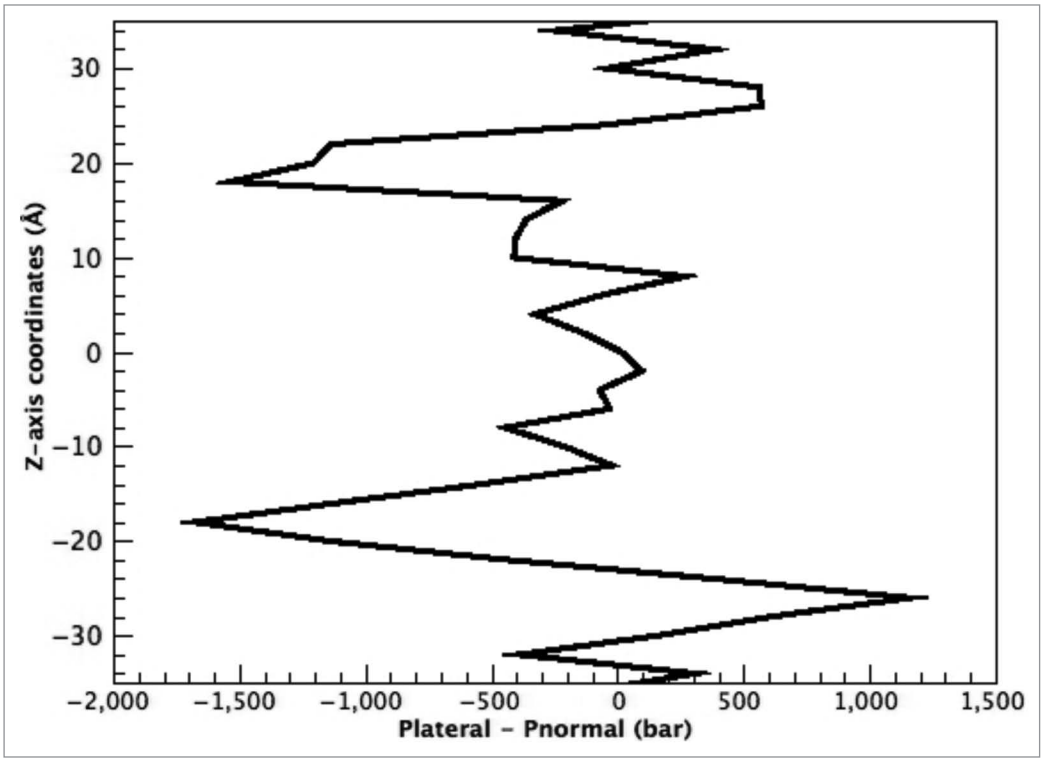

Figure 4. Pressure profile in the POPC lipid bilayer. Pressure in the membrane ($Pressure_{lateral}$ - $Pressure_{normal}$) is plotted against the transmembrane axis (z-axis), where the origin of the coordinates corresponds to the center of the membrane.

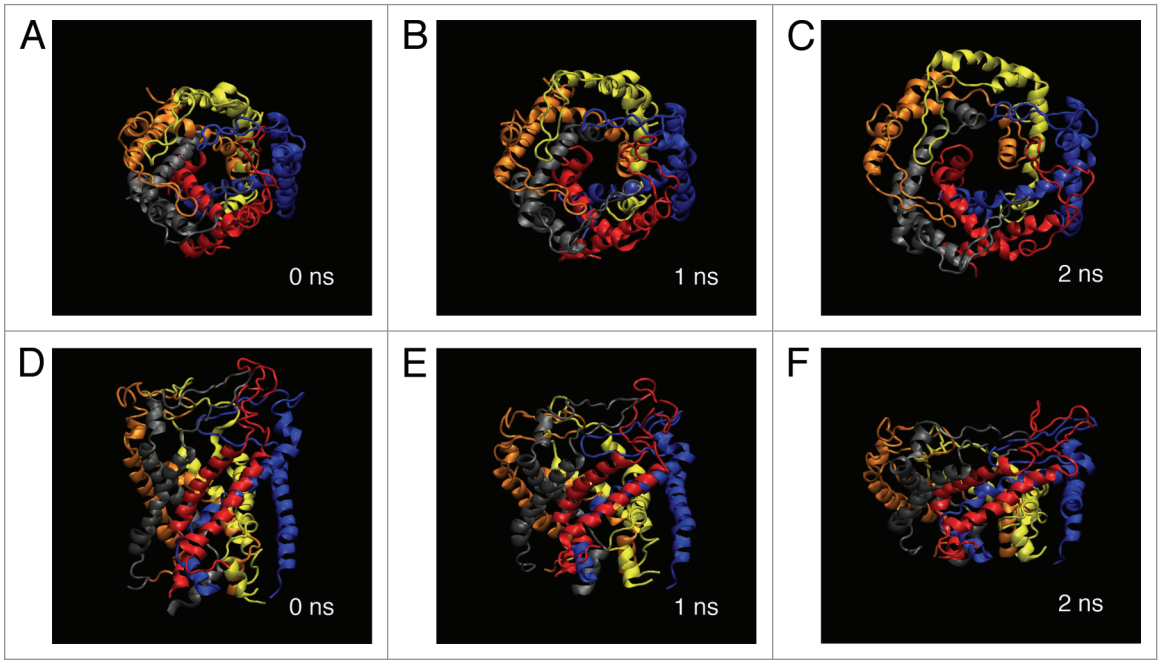

Figure 5. Snapshots of MscL structural changes upon tension increase. Top views taken at (**A**) 0 ns, (**B**) 1 ns and (**C**) 2 ns, and the corresponding side views (**D–F**). Eco-MscL is shown in a ribbon representation with different colors for each subunit. The lipid and water molecules are not shown here.

bilayer, RMSDs of the Cα atoms of the MscL protein were calculated during the equilibration process. **Figure 3** shows the time profile of RMSDs with respect to the Cα atoms during calculation relative to the initial structure. RMSDs during the preparation and annealing steps for modeling are not included in this figure. As shown, it is evident that at least 2 ns of equilibration were needed to stabilize the entire MscL structure.

Pressure profile of the POPC membrane under a potent stress. In the present study, to accelerate the structural changes induced by membrane tension increase we employed a much larger tension (150 dyn/cm) than (ca. 10 dyn/cm) used in usual experiments to activate MscL, which may disrupt the structure of the membrane.[6] In order to ascertain what happens in the bilayer structure under such a large stress, we calculated the pressure profile across the POPC membrane following the method used in earlier works.[22,38,39] As described in detail in the Materials and Methods section, the pressure profile across the lipid bilayer was obtained by calculating the local lateral pressure $P(z)$, defined as the difference between the normal and the lateral components of the pressure tensor P_{xx}, P_{yy} and P_{zz} in **Equation 1**. As given by **Equation 2**, the forces generated by stretching the membrane are estimated from the value of $P(z)$. **Figure 4** shows the pressure distribution in the membrane as a function of z-axis (transmembrane axis) coordinates calculated at the end of the POPC bilayer simulation (10 ns), in which the pressure profile have two distinct peaks around the glycerol moiety in the outer and inner leaflets of the POPC bilayer, respectively. This profile is essentially the same as that reported in earlier works, indicating that even under such a large negative pressure, the lipid bilayer retains its princip structure and physical properties and, thus, can mimic actual stretched membrane within our simulation time.[22,38,39]

Global structural changes in the MscL in response to membrane stretch. **Figure 5** shows a series of snap shots of structural changes in WT MscL in response to tension increase. During a 2 ns simulation, the transmembrane α-helices tilted and radially expanded in the membrane plane and the channel pore opened gradually. This is consistent with the suggestions reported in earlier studies.[41,42] **Table 1** shows the average radius (5.8 Å) of the most constricted part of the pore (the ostensible gate region of MscL) formed with the residues from Leu19 to Val23 in TM1 helix of each subunit at 2 ns simulation. However, this value (5.8 Å) is much smaller than the open pore size estimated by electrophysiological analyses or channel-mediated protein efflux measurements.[6,43,44] This suggests that the result here may reflect an initial conformational change on the way toward the full opening of MscL, which will be discussed later.

The expansion of the transmembrane region of MscL took place associated with tilting of the transmembrane helices toward the membrane plane, leading to a reduced MscL thickness. During the tilting process, the secondary structure of the transmembrane α-helices was partially degraded near the boundary region at the membrane/water interface, but the helical structure was essentially maintained during the simulation. This result indicates that the TM2 as well as TM1 helices are dragged by the force generated in the membrane and tilt down in order to maintain contact with the surrounding lipids while the membrane becomes thinner, suggesting that the received tension may be nearly directly conveyed to the gate region so as to induce channel opening. This opening process, which resembles the opening of an iris in a conventional optical camera, is consistent with earlier simulation results.[21,24,45]

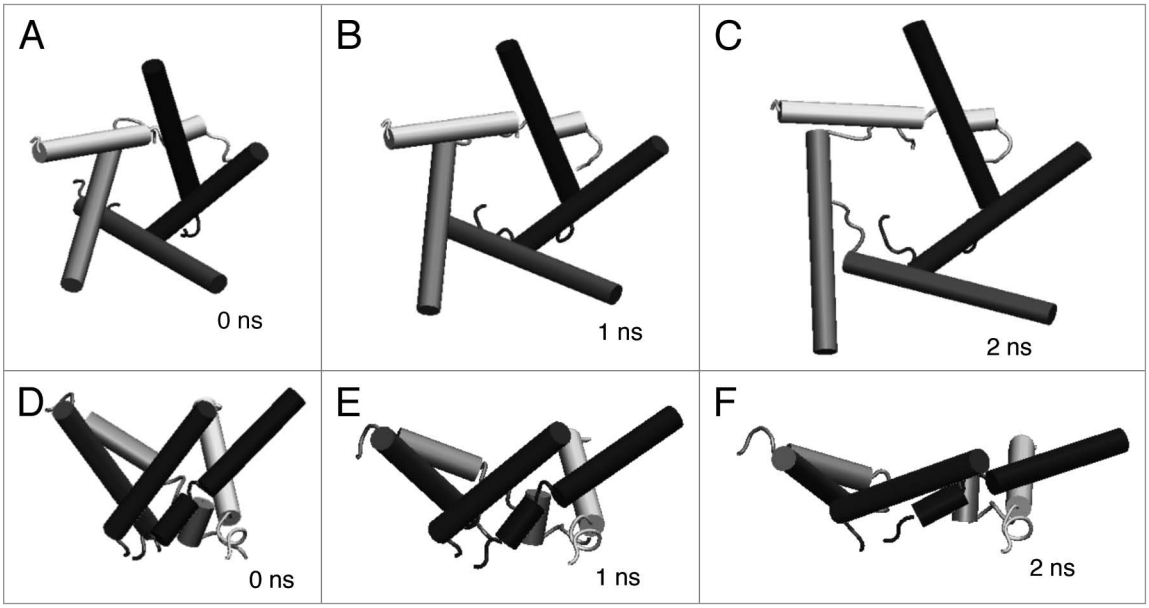

Figure 6. Snapshots of the configuration changes of the TM1 helices upon tension increase. Top views taken at (A) 0 ns, (B) 1 ns and (C) 2 ns, and the corresponding side views (D–F). TM1 helices in each snapshot are shown in a schematic representation with different colors for each subunit.

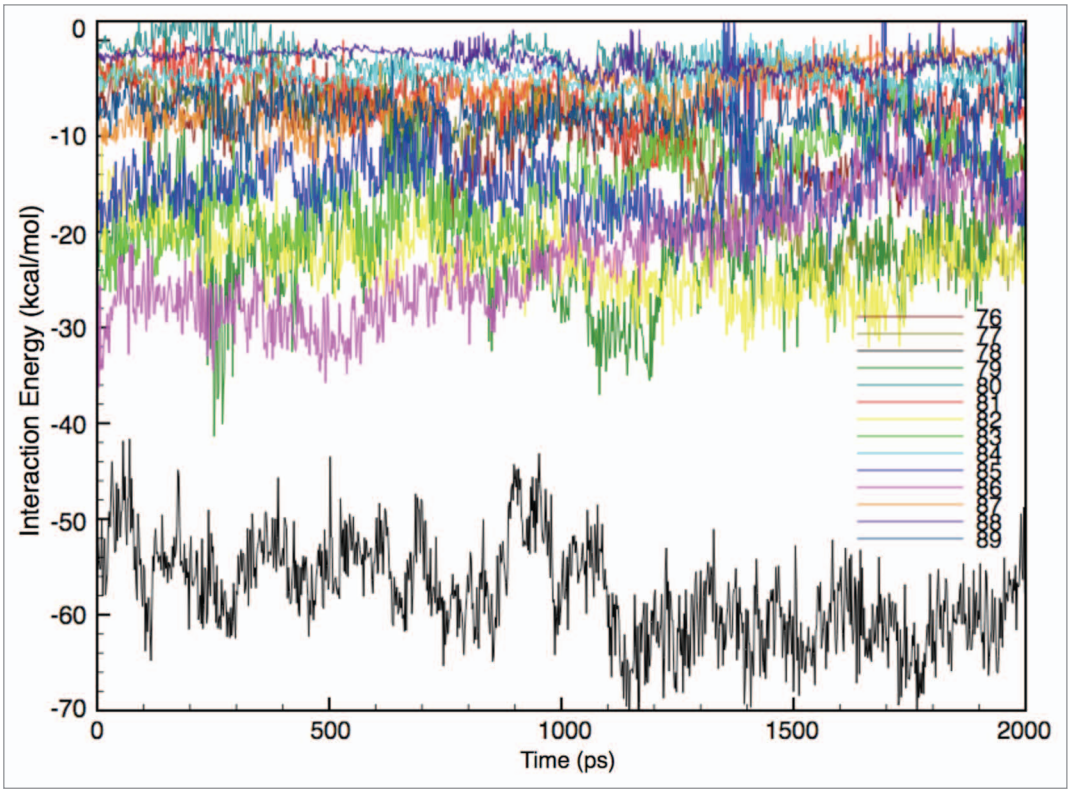

Figure 7. Time-course of the interaction energy between each amino acid (76–89) and the lipids upon tension increase. The interaction energy for each amino acid is depicted in a different color. The energy here consists of electrostatic and van der Waals interactions.

The initial structure of the MscL channel displayed rotational symmetry around the pore axis, but the channel expanded in an asymmetrical manner. As shown in **Figure 5**, one subunit expands more radially than other subunits after 2 ns of simulation. Such an asymmetrical feature of the movement of the helices can be seen more clearly in a series of snapshots of the configuration of the five inner (TM1) helices of the MscL during simulation (**Fig. 6**). TM1 helices tilted while sliding toward each

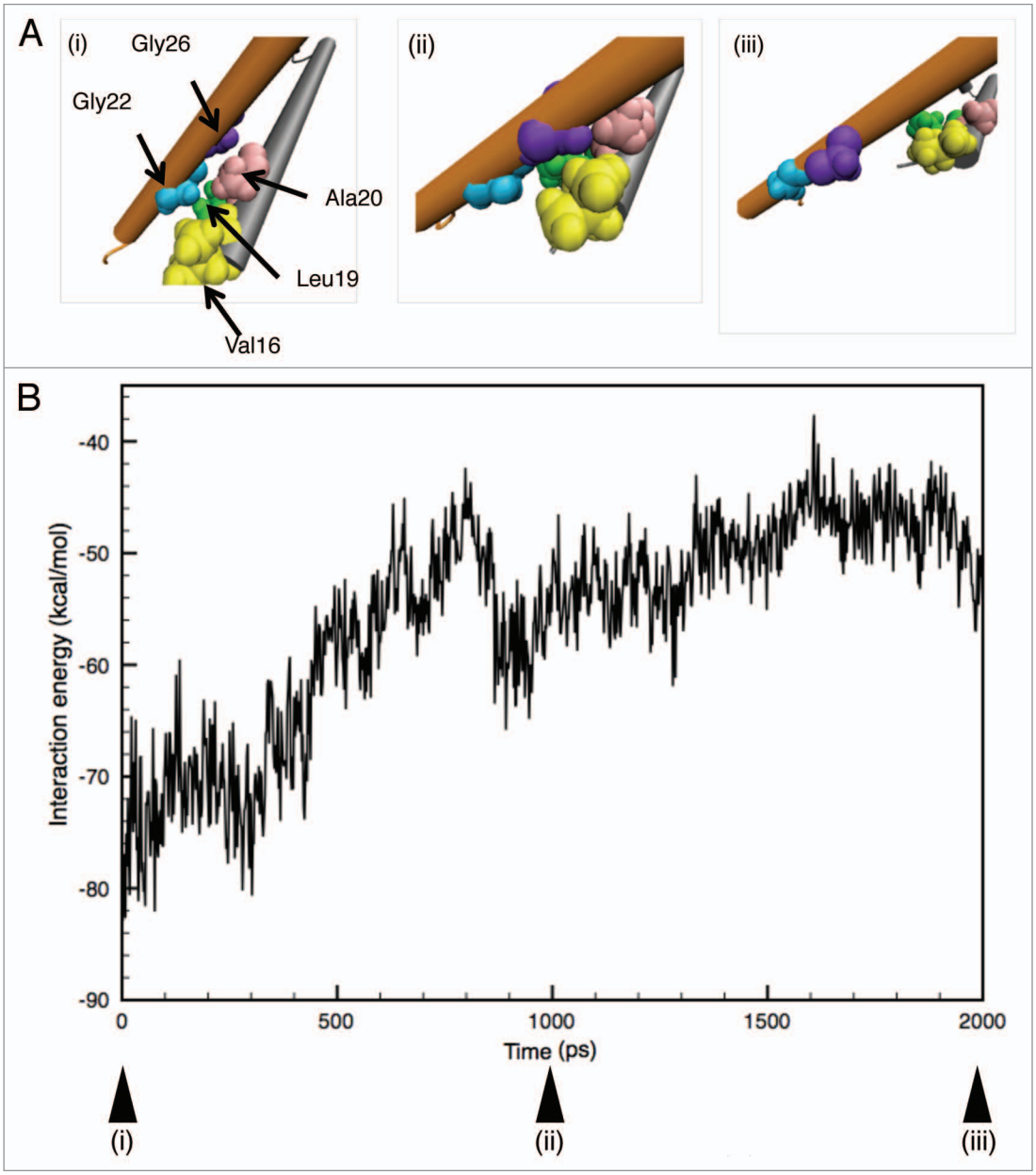

Figure 8. (**A**) Snapshots of the configuration changes of the crossing (interacting) portion formed by the two TM1 helices upon tension increase. Each panel represents the configuration at (i) 0, (ii) 1,000 and (iii) 2,000 ps of simulation, where Val16, Leu19, Ala20, Gly22 and Gly26 are shown in a yellow, green, pink, blue and purple colored VDW representation, respectively. (**B**) Time-course of the total interaction energy summed up from five crossing regions, in which (i), (ii) and (iii) are the same as described above.

other and expanded asymmetrically in a similar manner as TM2 helices. Essentially the same behavior of the asymmetrical opening of MscL was observed in the simulation by Rui et al. (2011).[46] Further details on this asymmetrical opening are described in the Discussion section.

Analysis of protein-lipid interactions: identification of tension sensor. MscL is a transmembrane protein lined with inner helices (TM1s) and surrounded by outer helices (TM2s), where TM2s form the major lipid-interacting region of MscL. The tilting down and radial expansion of the MscL subunits, shown in **Figures 5 and 6**, suggest that some of the amino acid residues located near the lipid water interface in the outer leaflet of the bilayer are strongly dragged by the adjacent lipids during the tension increase exerted by membrane stretching. In other words, these AAs are candidate tension-sensing sites of MscL, which is reasonable considering the fact that the strongest negative pressure (tension) across the membrane is generated near the lipid-water interface in the bilayer (**Fig. 4**). This is consistent with our earlier report suggesting that some of the amino acid residues near the periplasmic surface of the membrane are potential MscL tension-sensing sites.[15] To determine the major tension-sensing sites (tension sensor) in MscL, we estimated the interacting

energy between individual AA residues from Gly76 to Ala89 in TM2 helix and surrounding lipids. As these AAs maintained their interactions with lipid molecules during membrane stretching, we calculated the time profile of the interaction energies, as shown in **Figure 7**. The interaction energy was calculated based on electrostatic and van der Waals interactions, and the energy profile of each residue in **Figure 7** indicates the sum of the energies from five subunits. Surprisingly, the interaction energy between Phe78 and lipids is conspicuously much lower than that of any of other residues. That is, the interaction of Phe78 with lipids is much more specific compared with that of any other AA residues calculated. Since the tension sensitivity at the level of individual AA residues depends on the interaction between each AA and the lipids, Phe78 is thought to act as the major tension sensor of MscL.

Analysis of interactions between TM1 helices: gating process. The expansion of the most constricted part (gate) of the pore in **Figure 6** implies that the sliding of the interacting (crossing) site between neighboring TM1 helices is one of the barriers to the opening of MscL. In fact, it has been suggested that some of the residues around the crossing between TM1 helices behave as a barrier against channel opening.[21] In the present study, in order to know in detail how the gate region is expanded, we sought the AAs around the gate region responsible for the interaction between neighboring TM1 helices and found that, in the closed state, the residues (Val16, Leu19 and Ala20) on the TM1 helix come into contact with Gly22 and Gly26 on the neighboring TM1 helix while they are crossing each other. Gly22 began to come into contact with its neighboring TM1 helix in ~1 ns, fitting into a pocket formed by Val16, Leu19 and Ala20. After ~1 ns simulation, Gly26 instead of Gly22 began to come into contact with the residues forming the pocket [**Fig. 8A(i)–(iii)**]. This result is supported by an earlier work predicting that these interactions make the sliding motion of the TM1 helices less smooth.[21] We hypothesized that this corresponds to the first energy barrier on the way to full channel opening and calculated the interaction energy between the TM1 helices (as described in the Materials and Methods section) in order to compare it with that estimated by electrophysiology.[6] The calculated total interaction energy between TM1 helices as a function of time is shown in **Figure 8B**. The energy rises gradually until ~1 ns, followed by a transient drop, then gradually increases again, indicating that at least two energy states, separated by an energy barrier, exist during the 2 ns simulation. The energy difference between the two states was calculated to be ca. 25 kcal/mol (42 k_BT), with the energy of the first state determined as the average of the energy from 0–300 ps and that of the second state from 1,600–1,900 ps. An electrophysiological analysis estimated the free energy difference of MscL between the closed and the first subsonducting state to be ~38 k_BT.[6] Our calculation was made using just the local potential energy restricted to a region around the interacting sites of TM1 helices. It is rather surprising that such a limited calculation gives an energy value comparable to the experimentally estimated one.

Simulations of MscL mutants. As described above, our model, which is different from the previous models in terms of the method of applying forces to the channel, has qualitatively/semi-quantitatively reproduced the initial process of conformational changes toward the full opening of MscL in a similar manner reported earlier.[21,24,45] Furthermore, our results agree in principle with the proposed MscL gating models based on experiments.[42,47] However, it is unclear to what extent our model accurately simulates the mechano-gating of MscL. In order to evaluate the validity of our model, we examined the behaviors of the two MscL mutants F78N and G22N to test whether the mutant models would simulate their experimentally observed behaviors. These two mutants are known to open with greater difficulty (F78N) or ease (G22N) than WT MscL.[13,15,16,48]

Table 1 shows the values of the pore radius at 0 ns and 2 ns in the WT, and F78N and G22N mutant models calculated with the program HOLE.[40] The radii around the pore constriction region are evidently different between the WT and F78N mutant; the pore radius in the WT is ~5.8 Å, while that in the F78N mutant is ~3.3 Å. Comparing these two values, the F78N mutant seems to be consistent with the previous experimental result that F78N mutant is harder to open than WT and, thus, is called a "loss-of-function" mutant.[15] Furthermore, in order to determine what makes it harder for F78N-MscL to open than WT as a result of asparagine substitution, we calculated the interaction energy between Phe78 (WT) or Asn78 (F78N mutant) and the surrounding lipids. **Figure 9A** shows the time profile of the interaction energies of Phe78 (WT) and Asn78 (F78N mutant). Although the interaction energy between Asn78 and lipids is comparable with that of the Phe78-lipids until 1 ns, it gradually increases and the difference in the energy between them becomes significant at 2 ns simulation, demonstrating that this model does qualitatively simulate the F78N mutant behavior.

The gain-of-function mutant G22N, exhibits small conductance fluctuations even without membrane stretching.[16,48] We constructed a G22N mutant model and tested if it would reproduce this behavior by observing the conformational changes around the gate during 5 ns of equilibration without membrane stretching. **Figure 10A and B** show snapshots of the pore-constriction region around AA residue 22 and water molecules at 2 ns simulation for WT and G22N, respectively. In the WT model, there is virtually no water molecule in the gate region, probably because they are repelled from this region due to the hydrophobic nature of the gate region. By contrast, in the G22N mutant model, a significant number of water molecules are present in the gate region, which may represent a snapshot of the water permeation process. We compared the average pore radius in the gate region of the WT and G22N models at 2 ns. As shown in **Table 1**, the pore radius of the G22N mutant is significantly larger (3.8 Å) than that of the WT (1.9 Å), which is consistent with the above mentioned putative spontaneous water permeation observed in the G22N model.

Discussion

Aiming at identifying the tension-sensing site(s) and understanding the mechanisms of how the sensed force induces channel opening in MscL, we constructed molecular models for WT and mutant MscLs, and simulated the initial process of the channel

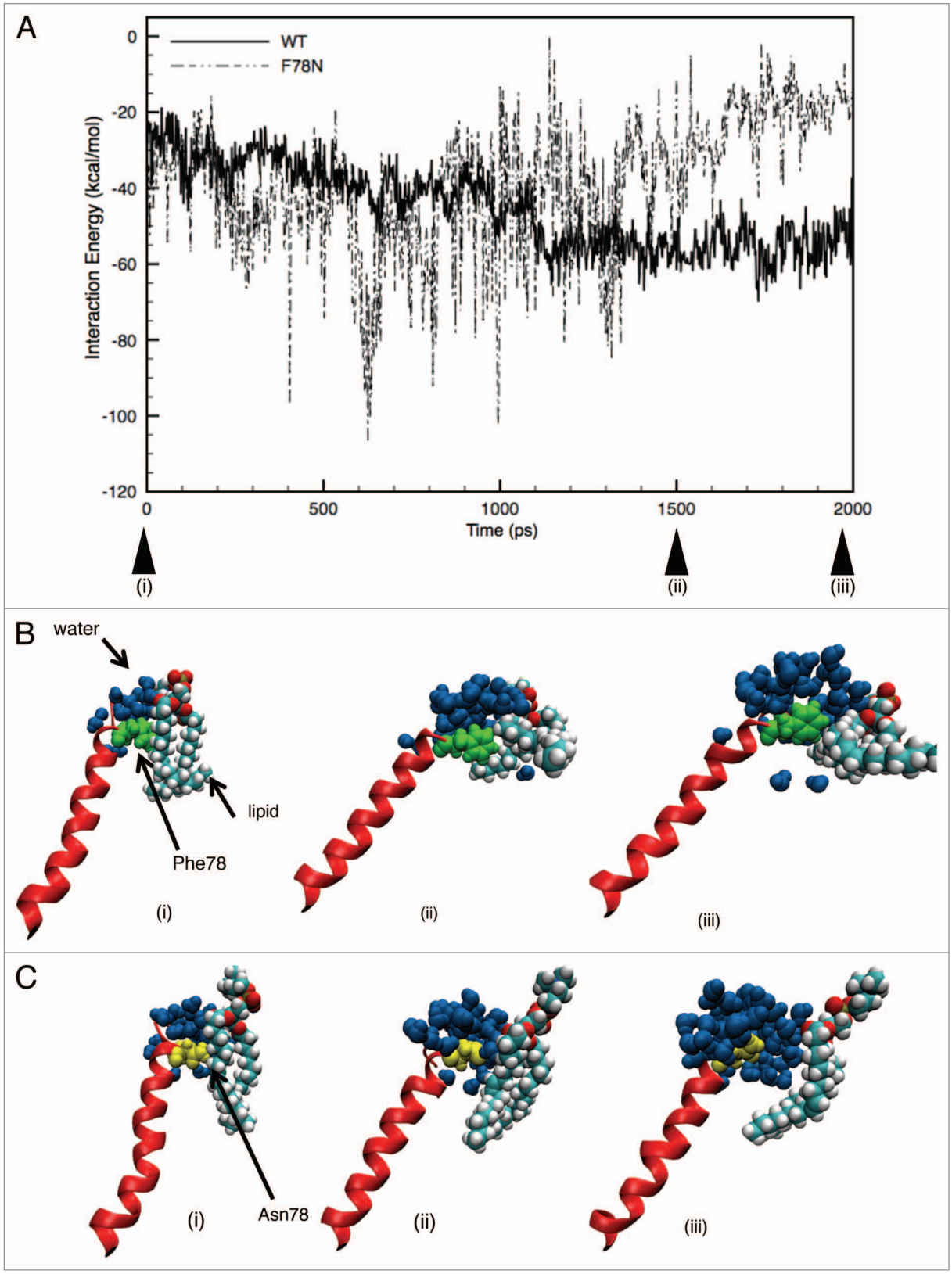

Figure 9. (**A**) Time-course of the changes in the interaction energy between Phe78 and the surrounding lipids upon tension increase. The interaction energy is the sum of that from five each of either Phe78-lipids or Asn78-lipids interactions at the corresponding TM1 helix in the WT (solid line) or F78N (dashed line) MscLs, respectively. The three upward arrowheads (i), (ii) and (iii) indicate the simulation time at 0, 1,500 and 2,000 ps, respectively. (**B and C**) Snapshots showing the protein-lipid-water boundary of the WT (**B**) and F78N (**C**) at 0 (i), 1,500 (ii) and 2,000 (iii) ps, respectively, where Phe78, Asn78 and water molecules are depicted in green, yellow and dark-blue colored VDW representations, respectively. A lipid molecule is shown in cyan (C atom), white (H atom), red (O atom), blue (N atom) and brown (P atom) colors, respectively.

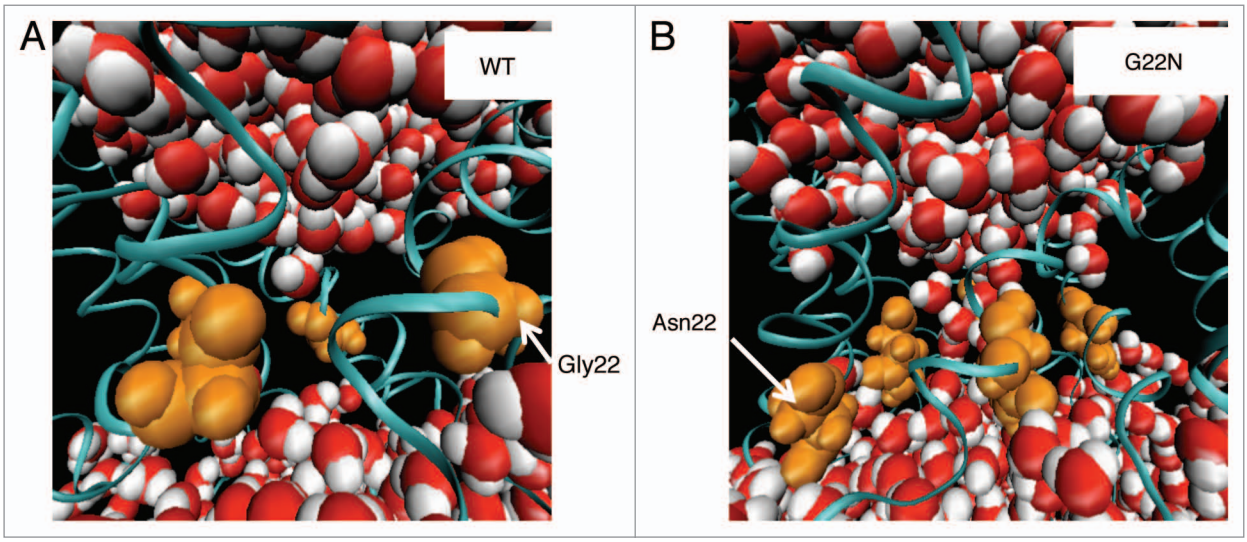

Figure 10. Conformation of the gate region of the WT and G22N MscLs. (**A**) WT and (**B**) G22N mutant at 2 ns of the equilibration simulation. Water molecules and the backbone Cα atoms of MscLs are depicted as VDW and ribbon representations, respectively. The five 22th amino acid residues of the WT (Gly) and G22N mutant (Asn) are shown as an orange VDW representation.

opening upon membrane stretch. The major results are as follows: (1) the AA Phe78 at the periplasmic surface on the outer helix TM2 was suggested to be the major tension-sensing site of MscL. This is based on the analysis of the interaction energy between individual AAs (Gly76 to Ala89) on TM2 and the lipids surrounding MscL; Phe78 showed conspicuously low interaction energy among the AAs. (2) TM1 helices, neighbors of which cross each other to form the pentagon-shaped gate of MscL in the inner leaflet of the bilayer, are dragged by the sensed force at Phe78 to expand the gate through a radial sliding of the crossing portions. The interaction energy at the crossing portions showed a jump at certain time point (ca. 0.8 ns, see **Fig. 8B**), the value for the energy jump is comparable to the experimentally estimated energy difference between the closed state and the first subconducting state of MscL. (3) The behaviors of the MscL mutant (F78N, G22N) models successfully mimicked the essential aspects of experimentally observed behaviors, supporting the validity of our MD model for WT MscL and obtained simulation results.

Protein-lipid interactions. Compositions of the lipid bilayer often affect the activity of membrane proteins, thus, many studies have been performed on the lipid-protein interaction.[49-52] The activation of bacterial MS channels, including MscL, is also critically dependent on the lipid-protein interaction, because these channels are activated exclusively by increased membrane tension that must be conveyed through mechanical coupling between the lipids immediately surrounding the channel protein and certain AA residues from the protein facing the lipids. If there is a particular AA that has a specifically strong interaction with the lipids, it can be defined as a tension sensor of the channel. As shown in **Figure 7**, Phe78 on the outer helix (TM2) of the MscL subunit was found to have a conspicuously strong interaction with lipids, among other AAs, strongly supporting the idea that Phe78 is the major tension sensor of MscL.

The most probable physicochemical mechanism for this strong interaction may be a CH/π interaction between the aromatic side chain of Phe78 and a CH_2 residue in the lipid acyl chains.[53,54] The aromatic side chain of Phe78 faced the CH_2 residues more frequently than the side chains of any other amino acids examined in our simulations. This is supported by the fact that among the aromatic residues, including Phe, Tyr, Trp and His, Phe exhibited the highest percentage of CH/π interaction.[54]

The Phe78-lipid interaction is apparently not the only mechanism involved in the MscL opening. At least strong interaction between TM2 and TM1 helices must be critical for the efficient transmission of the received force at Phe78 to the gate of MscL. To support this idea, asparagine substitution of some AAs in the region near the outer surface of the membrane of TM1 or TM2, or in the TM1-TM2 linker, decreases the sensitivity of MscL to membrane tension, resulting in loss-of-function mutants,[15] though the precise roles of these AAs await further investigation.

We also calculated the interaction energies between the AA residues 90–100 (located in the inner leaflet of the bilayer) of TM2 helix and surrounding lipids and found that only Lys97 had a much smaller value than any other AAs examined. However, there has been no report suggesting that Lys97 acts as a tension sensor. This AA may not be a tension sensor because the strong interaction is not stable during the course of membrane stretching; this point will be touched upon in detail later.

In this study, we analyzed the protein-lipid interactions under the membrane tension at 150 dyn/cm, which is approximately 10 times larger than that used in usual experiments. We examined whether such a strong tension affects the calculated energy value for the Phe78-lipid interaction under two other magnitudes of membrane tension (100 dyn/cm and no applied force). The calculated values under these conditions were nearly comparable to those at 150 dyn/cm, suggesting that the Phe78-lipid interaction

is mechanically very strong and stable, thus, eligible as a mechanosensing mechanism.

Asymmetric expansion of TM1/TM2 helices. As depicted in **Figures 5 and 6**, MscL opens its pore through tilting and sliding of TM1 helices in response to an increase in the membrane tension. This is realized by the radially directed dragging of the TM2/TM1 helices by the surrounding lipids. Interestingly, the dislocations of individual subunits (TM1/TM2) by the dragging were not uniform. Such asymmetrical movements of MscL subunits were also reported in an earlier simulation study.[46] One of the causes of the asymmetrical expansion of the helices may be the difference in the arrangement of the lipids around individual TM2 helcies. In fact, the number of interacting lipid molecules differed among TM2 helices and the values of the interaction energy between individual TM2 helices and the lipids were variable (data not shown). The lipids around MscL were arranged so as to stabilize MscL in the membrane during energy equilibrium calculations while each transmembrane helix retained its stability by interacting with a variety of moving and transforming lipids, resulting in a randomly fluctuating dynamic process. For example, Phe78 in TM2, which is supposed to act as the primary tension sensor, changes its interacting partner lipid(s) over time, in a manner that varied among the Phe78s in the five TM2s. This may account for the initiation of asymmetrical radial movements among TM2s. Once the stable interaction between neighboring TM1s is broken, radial movement of the interacting portion would be accelerated, resulting in more apparent asymmetrical expansion of the gate. Recent studies using disulfide cross-linking technique also suggest asymmetrical conformational changes among the MscL subunits during channel opening.[55,56]

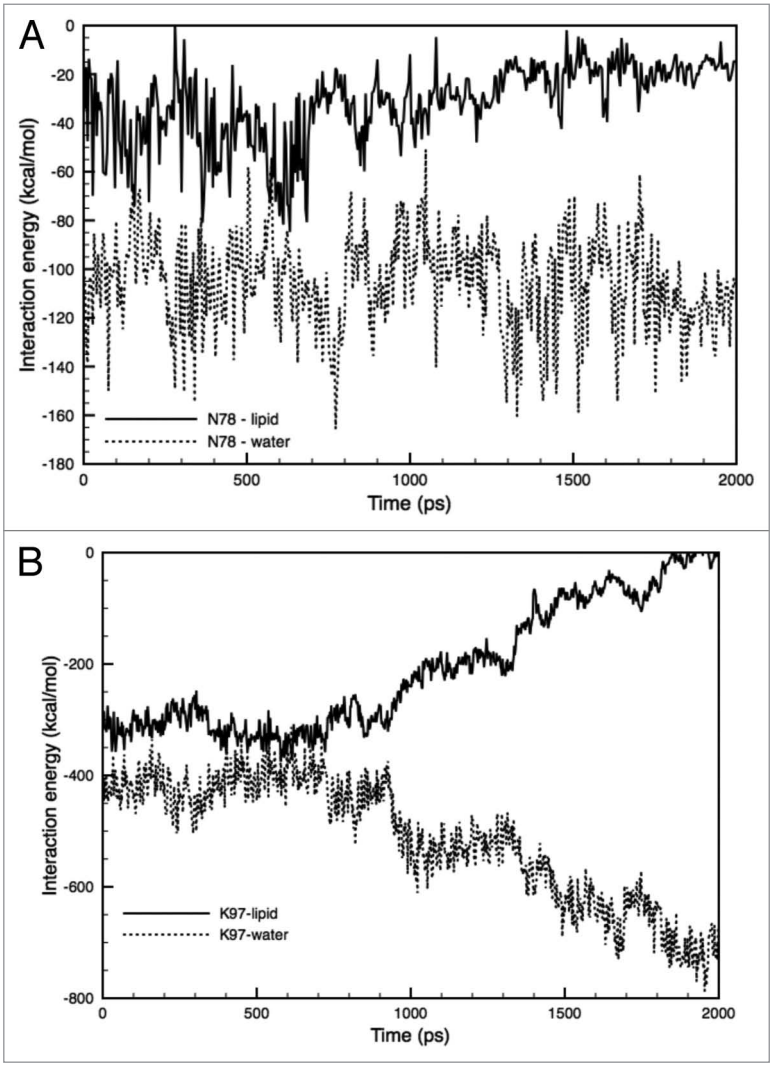

Figure 11. Time-course of the changes in the interaction energy between the hydrophilic (amino acid) AA residues and lipids/water. (**A**) Interaction energy between Asn78 and lipids (solid line), or water molecules (dotted line) in the F78N mutant. (**B**) Interaction energy between Lys97 and lipids (solid line), or water molecules (dotted line) in WT-MscL. Each energy profile is the sum of the interaction energy from five subunits.

Thermodynamic aspects of MscL opening. Sukharev et al. (1999) analyzed thermodynamic aspects of MscL gating based on the kinetics data on single-channel current fluctuations.[6] They found that at least five sub-conducting states exist and calculated the free energy differences between the states. The energy difference between the closed and the first sub-conducting state was ~38 k_BT, and the effective pore radius of the pore constriction region (gate) of MscL at the first sub-conducting state was approximately 4 Å.

In order to evaluate to what extent our simulations reproduce the experimentally estimated MscL features,[7] we calculated the energy changes during the course of MscL opening and obtained an energy difference between closed and putative first-transition state. The obtained value, approximately 25 kcal/mol (42 k_BT) in WT MscL, is comparable to the experimentally obtained value ca. 38 k_BT,[6] although our calculation was restricted to the energies at the interacting (crossing) portions between neighboring TM1s. Furthermore, the pore radius at the constriction region (gate) just after the apparent transition (ca. 1 ns) was calculated to be 3.9 Å, a value nearly the same as that of the experimentally estimated pore radius of the first sub-conducting state,[6] suggesting that our model could reproduce both the energetic and structural aspects of MscL features in the first opening step. As depicted in **Figure 8A**, the first transition may reflect the change in the binding partner of the gate forming AAs (Val16, Leu19 and Ala20) from Gyl22 to Gly26, whose process seems to be the major energy barrier for the transition, and corresponds to the energy peak at ca. 0.8 ns in **Figure 8B**.

Because of the methodological limitations, we calculated only the potential energies and compared them with free energies experimentally estimated. This may be rationalized by a recent study in which the free energy difference in the entire system, including lipids and water, between the closed and slightly open state of MscL, is of a comparable order with the value we obtained.[46] Another important point for the validity of our model, is that the MscL model maintained a relatively stable interaction with the lipid bilayer during the simulation as

demonstrated in the time profile of interaction energies between AAs (Gyl76-Ala89) on TM2s and lipids (**Fig. 7**).

What can we learn from the simulations on MscL mutants? One of the good tests for the validity of our MD simulation system is whether the model can successfully simulate the behaviors of some MscL mutants that show different modes of mechanogating in comparison with WT MscL. We employed two MscL mutants F78N and G22N, which are known to open less (F78N) and more (G22N) easily, respectively, than WT MscL.[15,16]

As mentioned, Phe78 is suspected to be the major tension sensor due to its conspicuous strong interaction with lipids. Therefore, "loss of function" mutant F78N was thought to be due to the loss of the strong interaction caused by the substitution of phenylalanine (Phe; F) to asparagine (Asn; N). Unexpectedly, however, the interaction energy between the Asn78 and lipids was comparable to that of Phe78 and lipids. The strong interaction was maintained until an elapsed time of 1 ns of simulation, however, it gradually decreased and the difference in the interaction between the Asn78-lipids and Phe78-lipids became significant at 2 ns (**Fig. 9A**). To determine what happens during this process, we compared the structure of the lipid-protein-water boundary in the WT and F78N simulations at 0, 1.5 and 2 ns, as shown in **Figure 9B and C**. At the starting point (0 ns) of the simulation, WT and F78N did not have any gap between the 78th amino acid and adjacent lipids. However, as shown in **Figure 9C**, (ii), a gap between Asn78 and the lipids was created and water molecules penetrated into the gap after 1.5 ns in the F78N mutant, whereas there was no gap between Phe78 and the lipids in the WT MscL [**Fig. 9B**, (ii)]. After 2 ns, the gap between the Asn78 and the lipids in the F78N became wider and many more water molecules penetrated into the gap [**Fig. 9C**, (iii)], while there was still no gap between the Phe78 and the lipids in WT [**Fig. 9B**, (iii)]. We do not know the details of the water penetration process, however, it can be speculated that spatial fluctuations in the gap trigger the water penetration and that it proceeds in F78N due to the hydrophilic nature of asparagines (Asn; N). On the other hand, in the case of WT (Phe78), water penetration will not proceed due to the hydrophobic nature of phenylalanine. The time profiles of N78-lipids and N78-water interactions in **Figure 11A** clearly show that N78-water interaction is evidently stronger than N78-lipid interaction, suggesting that there is a good chance for water penetration into the gap between Asn78 and lipids during the spatial fluctuations of the gap as demonstrated in **Figure 9C**, (iii). As the result, TM2 helix in the F78N mutant tilts much less compared with the WT MscL [compare **Fig. 9C and B**, (iii) and (iii)].

Interestingly, a similar phenomenon was observed in the Lys97-lipid-water boundary in the WT MscL. As mentioned in the Results section, Lys97 has strong interaction with lipids, but as shown in **Figure 11B**, after the onset of tension increase, the Lys97-lipid interaction became unstable at approximately 1 ns of simulation. On the other hand, the Lys97-water interaction became much more stable than the Lys97-lipid interaction. A tension increase may trigger and increase the gap between Lys97 and lipids, allowing the penetration of water molecules. Taken together, although Lys97 in the WT and F78N MscLs and Asn78 in F78N MscL have strong interactions with lipids comparable to the Phe78 in WT, these two residues cannot maintain a stable strong interaction with lipids under a condition with increased membrane tension due to their hydrophilic nature. Thus, not only a strong interaction with lipids, but also its stability under increased tension, may be a critical requirement of amino acids to be a tension sensor.

As the G22N mutant exhibits spontaneous channel opening without any increased membrane tension,[16,48] we performed a simulation of the G22N mutant without applying negative lateral pressure to the membrane. As seen in **Figure 10**, this MscL mutant seems to permeate water molecules across the pore without increased tension in the membrane, while this is not the case in the WT MscL. These results suggest that the G22N mutant has a hydrophilic environment around the gate region due to the hydrophilic side chains of the asparagine residues, which may not give rise to the hydrophobic environment called "vapor lock" that blocks the permeation of water and ions in the WT MscL.[57] Furthermore, the resulting hydration around the gate of the G22N mutant as well as steric hindrance due to larger residue size of asparagine, seemed to induce a slight opening of the gate, probably through weakening the hydrophobic lock, which is originally created by the interaction between Gly22 and a group of hydrophobic amino residues (Val16, Leu19 and Ala20) in the WT MscL (see **Fig. 8**). This may account for the observed spontaneous channel opening and the lower threshold to open the channel in the G22N mutant.[16]

Materials and Methods

System setup for simulation. The original Eco-MscL structure, which is based on the crystal structure of Tb-MscL, was used in this study.[5] It was originally modeled in an earlier work and is provided at the author's website.[29] The residues in the cytoplasmic region beyond Ala110 of the Eco-MscL, which have been suggested to not be essential for MscL gating, have been excised to reduce the total size of the system.[30] A pre-equilibrated palmitoyl-oleoyl-phosphatidylcholine (POPC) bilayer was modeled with the molecular graphics program VMD.[31] The membrane was oriented in the xy plane with a size of 100 Å × 100 Å, with the z axis as the membrane normal. Then an Eco-MscL model was embedded by superimposing the channel structure onto the membrane, followed by removal of the lipids located within the pore region and extensively overlapped with the channel using tcl script. A large number of water molecules were placed 10 Å above and below the membrane. The simple point charge (SPC) water molecule model was used with the SOLVATE program.[32] The total simulation system consisted of an Eco-MscL protein, 128 lipid molecules and 19,000 water molecules, having 95,175 atoms and ~10 nm × 10 nm × 10.5 nm in the initial dimensions (**Fig. 2**). Energy minimization was performed to remove bad contacts and then the energy-minimized system was equilibrated at 1 atm, 310 K, for 3 ns. Although the 3 ns of the equilibration time is shorter than generally reported ones, we confirmed that our simulation results did not change regardless of the period of the equilibration time, if it is 3 ns or longer.

Computational details. All simulations were performed using the program NAMD 2.6 together with the CHARMM force field for proteins and lipids under a three-dimensional periodic boundary condition, full electrostatics with PME and a cutoff for van der Waals interactions at 12 Å.[33-36] The density of the grid points for PME was at least 1/Å in all cases. In the MscL opening simulations, a negative pressure at 150 dyn/cm was generated only in the lateral axis in the membrane while a constant pressure of 1 bar was set in the z-direction. The rest of the components of the system, including the bulk water and MscL proteins, were not subjected to the negative pressure. This protocol for generating negative pressure in the membrane was used with the description included in an input file, while the components, except for the membrane, were defined in an additional file. The negative lateral pressure in the lipid bilayer is considered to mimic the stretched membrane used in patch-clamp experiments.[6,37]

Calculation of transmembrane pressure profile. In order to determine whether this method for applying negative pressure to the membrane retains the original features without the intrusion of any fatal artifacts, we calculated a pressure profile of the membrane with the method proposed in an earlier work.[22] First, we performed a 10 ns equilibrating simulation of a POPC bilayer (without MscL), followed by a simulation for 3 ps under the condition of 150 dyn/cm membrane tension. Then the diagonal components of pressure tensor were computed in the stretched membrane and saved every 100 fs in the last 2 ps of the simulation. With this protocol, we described 20 pressure profiles as a function of the transmembrane axis coordinates and finally the pressure profiles at each time step were summed and averaged over the entire 20 profiles.

In earlier studies, the pressure profile across the lipid bilayer was characterized by two peaks of negative pressure (tension) near lipid-water interfaces.[38,39] In the calculation, the local lateral pressure $P(z)$ is defined as the difference between the normal and the lateral components of the pressure tensor as $P(z) = (P_{xx} + P_{yy})/2 - P_{zz}$, (**Eqn. 1**) where P_{xx}, P_{yy} and P_{zz} are the x, y and z diagonal components of the pressure tensor,[39] which are given by

$$p_{xx} = \frac{1}{\Delta V}\sum F_x r_x \quad \text{(Eqn. 2)}.$$

Calculation of interaction energies. In order to quantitatively analyze the gating properties of MscL, we calculated the interaction energies between three different pairs, MscL-surrounding lipids, AA residues-lipids and TM1-TM1 helices, using the NAMDEnergy program, one of the VMD plug-ins.[31] The NAMDEnergy plug-in can provide the energies of selected atoms, residues and subunits in each simulation step. The interaction energies calculated in this study include both electrostatic and van der Waals interactions. All of the energy profiles shown here are the sum of the values of these interaction energies. As for the interaction energy between TM1 helices, we first calculated the energy for each of 5 TM1s from five subunits of MscL and obtained values were summed up, and then divided by 2. This is because each TM1 helix interacts with both the left and right neighbors and simple summation gives a doubled value of the correct total energy.

Modeling of MscL mutants. In order to evaluate this model system, including the MscL channel, lipid bilayer and the generation of tension, we modeled two MscL mutants and examined whether their calculated gating behaviors are consistent with the experimental results. The two mutants F78N and G22N, which reportedly are harder (loss-of-function) or easier to open (gain-of-function) than the WT, were made by substituting phenylalanine (Phe78) or glycine (Gly22) with asparagines (Asn, N), respectively, using the mutant modeling tool in VMD.[31] Energy minimization was performed for 2,000 steps in each system after the modeling to remove bad contacts, especially around the substituted residue, then equilibrium calculations were performed until the root mean square deviation (RMSD) value for the Cα atoms of the mutant MscL became nearly constant. One ns of calculation time was needed to obtain equilibration for the F78N mutant and 1.5 ns for the G22N mutant. MD simulations of the two mutants were performed under the same conditions as that of the WT MscL simulation except for the applied tension to the G22N mutant. Simulations for the G22N mutant was performed without applying negative pressure and only during the equilibrating calculation for 5 ns, because the G22N mutant undergoes spontaneous opening without mechanical stimulation (membrane stretch).[13,16]

Estimation of the pore size. The minimum pore radius of MscL was calculated by the HOLE program using a spherical probe.[40] At 2 ns, the coordinate of the channel was exported to a file in PDB format containing the Cartesian coordinates of the atoms on VMD and the pore dimension was calculated with its coordinates.[31] In this study, a vector normal to the membrane plane from the median point of the pore was defined as the channel axis and the pore radius was calculated as the average distance from the channel axis to the internal surface of the pore. After the loading of the HOLE program, calculations of the pore radius were performed by running the tcl script on VMD. In the present study, pore radii were calculated in the plane where AA 22 (G22) is located, which has been suggested to be the most constricted part of the pore called gate.[13]

Conclusions

Our MD simulations of the MscL gating have demonstrated that tension increase in the bilayer results in tilting of the transmembrane helices and expansion of the gate through radial drag of certain hydrophobic amino acid residue(s) by the immediately surrounding lipids. Calculations of the interaction energies between the lipids and individual amino acid residues on TM2 facing the lipids demonstrated that Phe78, located near the periplasmic membrane surface, has a conspicuously strong interaction with the lipids, thus, it was concluded that Phe78 is the primary MscL tension sensor. The gate expansion caused by the radial dragging of the helices is realized by a radial sliding of the interacting portions between neighboring TM1s. The time profile of this interaction energy is separated by an energy peak and the difference in the energies separated by the peak is comparable to the experimentally estimated value of energy jump from the closed to the first sub-conductance state, suggesting

that our simulation mimics the initial step of the channel gating toward the full opening of MscL. Successful simulations of the behaviors of the GOF (G22N) and LOF (F78N) mutants with our MD model system demonstrates its high validity to simulate the WT MscL gating process. Thus, it would be a valuable challenge to examine with this model the effects of generic gating modifiers, such as lyso- or short-chain lipids, or amphipaths on the MscL gating, which would give further insights into the underlying biophysical mechanism of mechanogating in the MS channels activated by membrane tension.

Disclosure of Potential Conflicts of Interest

No potential conflicts of interest were disclosed.

Acknowledgments

This work was supported in part by grants-in-aid from the Ministry of Education Science Sports and Culture: General Scientific Research (13480216 to M.S.); Scientific Research on Priority Areas (15086270 to M.S.); Creative Research (16GS0308 to M.S.) and by a grant from the Japan Space Forum (to M.S.).

References

1. Hamill OP, Martinac B. Molecular basis of mechanotransduction in living cells. Physiol Rev 2001; 81:685-740; PMID:11274342.
2. Levina N, Tötemeyer S, Stokes NR, Louis P, Jones MA, Booth IR. Protection of *Escherichia coli* cells against extreme turgor by activation of MscS and MscL mechanosensitive channels: identification of genes required for MscS activity. EMBO J 1999; 18:1730-7; PMID:10202137; http://dx.doi.org/10.1093/emboj/18.7.1730.
3. Batiza AF, Kuo MM-C, Yoshimura K, Kung C. Gating the bacterial mechanosensitive channel MscL *invivo.* Proc Natl Acad Sci USA 2002; 99:5643-8; PMID:11960017; http://dx.doi.org/10.1073/pnas.082092599.
4. Sukharev SI, Blount P, Martinac B, Blattner FR, Kung C. A large-conductance mechanosensitive channel in E. coli encoded by mscL alone. Nature 1994; 368:265-8; PMID:7511799; http://dx.doi.org/10.1038/368265a0.
5. Chang G, Spencer RH, Lee AT, Barclay MT, Rees DC. Structure of the MscL homolog from *Mycobacterium tuberculosis*: a gated mechanosensitive ion channel. Science 1998; 282:2220-6; PMID:9856938; http://dx.doi.org/10.1126/science.282.5397.2220.
6. Sukharev SI, Sigurdson WJ, Kung C, Sachs F. Energetic and spatial parameters for gating of the bacterial large conductance mechanosensitive channel, MscL. J Gen Physiol 1999; 113:525-40; PMID:10102934; http://dx.doi.org/10.1085/jgp.113.4.525.
7. Sukharev S, Betanzos M, Chiang CS, Guy HR. The gating mechanism of the large mechanosensitive channel MscL. Nature 2001; 409:720-4; PMID:11217861; http://dx.doi.org/10.1038/35055559.
8. Sokabe M, Sachs F, Jing ZQ. Quantitative video microscopy of patch clamped membranes stress, strain, capacitance, and stretch channel activation. Biophys J 1991; 59:722-8; PMID:1710939; http://dx.doi.org/10.1016/S0006-3495(91)82285-8.
9. Moe P, Blount P. Assessment of potential stimuli for mechano-dependent gating of MscL: effects of pressure, tension, and lipid headgroups. Biochemistry 2005; 44:12239-44; PMID:16142922; http://dx.doi.org/10.1021/bi0509649.
10. Moe PC, Levin G, Blount P. Correlating a protein structure with function of a bacterial mechanosensitive channel. J Biol Chem 2000; 275:31121-7; PMID:10846181; http://dx.doi.org/10.1074/jbc.M002971200.
11. Steinbacher S, Bass R, Strop P, Rees DC. Structures of the prokaryotic mechanosensitive channels MscL and MscS. In: Part A, Simon S, Hamill O, Benos D, eds. Mechanosensitive Ion Channels. San Diego: Elsevier Academic Press Inc, 2007:1–24.
12. Sukharev S, Durell SR, Guy HR. Structural models of the MscL gating mechanism. Biophys J 2001; 81:917-36; PMID:11463635; http://dx.doi.org/10.1016/S0006-3495(01)75751-7.
13. Yoshimura K, Batiza A, Schroeder M, Blount P, Kung C. Hydrophilicity of a single residue within MscL correlates with increased channel mechanosensitivity. Biophys J 1999; 77:1960-72; PMID:10512816; http://dx.doi.org/10.1016/S0006-3495(99)77037-2.
14. Yoshimura K, Batiza A, Kung C. Chemically charging the pore constriction opens the mechanosensitive channel MscL. Biophys J 2001; 80:2198-206; PMID:11325722; http://dx.doi.org/10.1016/S0006-3495(01)76192-9.
15. Yoshimura K, Nomura T, Sokabe M. Loss-of-function mutations at the rim of the funnel of mechanosensitive channel MscL. Biophys J 2004; 86:2113-20; PMID:15041651; http://dx.doi.org/10.1016/S0006-3495(04)74270-8.
16. Yoshimura K, Usukura J, Sokabe M. Gating-associated conformational changes in the mechanosensitive channel MscL. Proc Natl Acad Sci USA 2008; 105:4033-8; PMID:18310324; http://dx.doi.org/10.1073/pnas.0709436105.
17. Maurer JA, Dougherty DA. Generation and evaluation of a large mutational library from the *Escherichia coli* mechanosensitive channel of large conductance, MscL: implications for channel gating and evolutionary design. J Biol Chem 2003; 278:21076-82; PMID:12670944; http://dx.doi.org/10.1074/jbc.M302892200.
18. Ou X, Blount P, Hoffman RJ, Kung C. One face of a transmembrane helix is crucial in mechanosensitive channel gating. Proc Natl Acad Sci USA 1998; 95:11471-5; PMID:9736761; http://dx.doi.org/10.1073/pnas.95.19.11471.
19. Blount P, Sukharev SI, Schroeder MJ, Nagle SK, Kung C. Single residue substitutions that change the gating properties of a mechanosensitive channel in *Escherichia coli.* Proc Natl Acad Sci USA 1996; 93:11652-7; PMID:8876191; http://dx.doi.org/10.1073/pnas.93.21.11652.
20. Gullingsrud J, Kosztin D, Schulten K. Structural determinants of MscL gating studied by molecular dynamics simulations. Biophys J 2001; 80:2074-81; PMID:11325711; http://dx.doi.org/10.1016/S0006-3495(01)76181-4.
21. Gullingsrud J, Schulten K. Gating of MscL studied by steered molecular dynamics. Biophys J 2003; 85:2087-99; PMID:14507677; http://dx.doi.org/10.1016/S0006-3495(03)74637-2.
22. Gullingsrud J, Schulten K. Lipid bilayer pressure profiles and mechanosensitive channel gating. Biophys J 2004; 86:3496-509; PMID:15189849; http://dx.doi.org/10.1529/biophysj.103.034322.
23. Elmore DE, Dougherty DA. Molecular dynamics simulations of wild-type and mutant forms of the Mycobacterium tuberculosis MscL channel. Biophys J 2001; 81:1345-59; PMID:11509350; http://dx.doi.org/10.1016/S0006-3495(01)75791-8.
24. Colombo G, Marrink SJ, Mark AE. Simulation of MscL gating in a bilayer under stress. Biophys J 2003; 84:2331-7; PMID:12668441; http://dx.doi.org/10.1016/S0006-3495(03)75038-3.
25. Meyer GR, Gullingsrud J, Schulten K, Martinac B. Molecular dynamics study of MscL interactions with a curved lipid bilayer. Biophys J 2006; 91:1630-7; PMID:16751236; http://dx.doi.org/10.1529/biophysj.106.080721.
26. Debret G, Valadié H, Stadler AM, Etchebest C. New insights of membrane environment effects on MscL channel mechanics from theoretical approaches. Proteins 2008; 71:1183-96; PMID:18004782; http://dx.doi.org/10.1002/prot.21810.
27. Jeon J, Voth GA. Gating of the mechanosensitive channel protein MscL: the interplay of membrane and protein. Biophys J 2008; 94:3497-511; PMID:18212020; http://dx.doi.org/10.1529/biophysj.107.109850.
28. Louhivuori M, Risselada HJ, van der Giessen E, Marrink SJ. Release of content through mechano-sensitive gates in pressurized liposomes. Proc Natl Acad Sci USA 2010; 107:19856-60; PMID:21041677; http://dx.doi.org/10.1073/pnas.1001316107.
29. Gullingsrud J, Sotomayor M. 2003. The structure file of MscL. http://www.ks.uiuc.edu/Research/MscLchannel/
30. Ajouz B, Berrier C, Besnard M, Martinac B, Ghazi A. Contributions of the different extramembranous domains of the mechanosensitive ion channel MscL to its response to membrane tension. J Biol Chem 2000; 275:1015-22; PMID:10625640; http://dx.doi.org/10.1074/jbc.275.2.1015.
31. Humphrey W, Dalke A, Schulten K. VMD: visual molecular dynamics. J Mol Graph 1996; 14:33-8, 27-8; PMID:8744570; http://dx.doi.org/10.1016/0263-7855(96)00018-5.
32. Grubmüller H. 1996. SOLVATE 1.0. http://www.mpibpc.gwdg.de/ abteilungen/071/solvate/docu.html.
33. Kale L, Skeel R, Bhandarkar M, Brunner R, Gursoy A, Krawetz N, et al. NAMD2: greater scalability for parallel molecular dynamics. J Comput Phys 1999; 151:283-312; http://dx.doi.org/10.1006/jcph.1999.6201.
34. MacKerell AD Jr., Bashford D, Bellott M, Dunbrack RL Jr., Evanseck J, Field MJ, et al. All-hydrogen empirical potential for molecular modeling and dynamics studies of proteins using the CHARMM22 force field. J Phys Chem B 1998; 102:3586-616.
35. Schlenkrich M, Brickmann J, MacKerell AD Jr., Karplus M. Empirical potential energy function for phospholipids: criteria for parameter optimization and applications. In: Merz K M, Roux B, eds. Biological Membranes: A Molecular Perspective from Computation and Experiment. Boston: Birkhauser, 1996:31– 81.
36. Darden T, York D, Pedersen L. Particle Mesh Ewald - an N.Log(N) method for Ewald sums in large systems. J Chem Phys 1993; 98:10089-92; http://dx.doi.org/10.1063/1.464397.
37. Häse CC, Le Dain AC, Martinac B. Purification and functional reconstitution of the recombinant large mechanosensitive ion channel (MscL) of *Escherichia coli.* J Biol Chem 1995; 270:18329-34; PMID:7543101; http://dx.doi.org/10.1074/jbc.270.31.18329.

38. Cantor RS. The lateral pressure profile in membranes: a physical mechanism of general anesthesia. Biochemistry 1997; 36:2339-44; PMID:9054538; http://dx.doi.org/10.1021/bi9627323.
39. Lindahl E, Edholm O. Mesoscopic undulations and thickness fluctuations in lipid bilayers from molecular dynamics simulations. Biophys J 2000; 79:426-33; PMID:10866968; http://dx.doi.org/10.1016/S0006-3495(00)76304-1.
40. Smart OS, Neduvelil JG, Wang X, Wallace BA, Sansom MSP. HOLE: a program for the analysis of the pore dimensions of ion channel structural models. J Mol Graph 1996; 14:354-60, 376; PMID:9195488; http://dx.doi.org/10.1016/S0263-7855(97)00009-X.
41. Betanzos M, Chiang CS, Guy HR, Sukharev S. A large iris-like expansion of a mechanosensitive channel protein induced by membrane tension. Nat Struct Biol 2002; 9:704-10; PMID:12172538; http://dx.doi.org/10.1038/nsb828.
42. Perozo E, Cortes DM, Sompornpisut P, Kloda A, Martinac B. Open channel structure of MscL and the gating mechanism of mechanosensitive channels. Nature 2002; 418:942-8; PMID:12198539; http://dx.doi.org/10.1038/nature00992.
43. Cruickshank CC, Minchin RF, Le Dain AC, Martinac B. Estimation of the pore size of the large-conductance mechanosensitive ion channel of *Escherichia coli*. Biophys J 1997; 73:1925-31; PMID:9336188; http://dx.doi.org/10.1016/S0006-3495(97)78223-7.
44. van den Bogaart G, Krasnikov V, Poolman B. Dual-color fluorescence-burst analysis to probe protein efflux through the mechanosensitive channel MscL. Biophys J 2007; 92:1233-40; PMID:17142294; http://dx.doi.org/10.1529/biophysj.106.088708.
45. Yefimov S, van der Giessen E, Onck PR, Marrink SJ. Mechanosensitive membrane channels in action. Biophys J 2008; 94:2994-3002; PMID:18192351; http://dx.doi.org/10.1529/biophysj.107.119966.
46. Rui H, Kumar R, Im W. Membrane tension, lipid adaptation, conformational changes, and energetics in MscL gating. Biophys J 2011; 101:671-9; PMID:21806935; http://dx.doi.org/10.1016/j.bpj.2011.06.029.
47. Kong Y, Shen Y, Warth TE, Ma J. Conformational pathways in the gating of Escherichia coli mechanosensitive channel. Proc Natl Acad Sci USA 2002; 99:5999-6004; PMID:11972047; http://dx.doi.org/10.1073/pnas.092051099.
48. Anishkin A, Chiang CS, Sukharev S. Gain-of-function mutations reveal expanded intermediate states and a sequential action of two gates in MscL. J Gen Physiol 2005; 125:155-70; PMID:15684093; http://dx.doi.org/10.1085/jgp.200409118.
49. Tieleman DP, Forrest LR, Sansom MS, Berendsen HJ. Lipid properties and the orientation of aromatic residues in OmpF, influenza M2, and alamethicin systems: molecular dynamics simulations. Biochemistry 1998; 37:17554-61; PMID:9860871; http://dx.doi.org/10.1021/bi981802y.
50. Dumas F, Lebrun MC, Tocanne JF. Is the protein/lipid hydrophobic matching principle relevant to membrane organization and functions? FEBS Lett 1999; 458:271-7; PMID:10570923; http://dx.doi.org/10.1016/S0014-5793(99)01148-5.
51. Mouritsen OG, Bloom M. Mattress model of lipid-protein interactions in membranes. Biophys J 1984; 46:141-53; PMID:6478029; http://dx.doi.org/10.1016/S0006-3495(84)84007-2.
52. Mouritsen OG, Bloom M. Models of lipid-protein interactions in membranes. Annu Rev Biophys Biomol Struct 1993; 22:145-71; PMID:8347987; http://dx.doi.org/10.1146/annurev.bb.22.060193.001045.
53. Tsuzuki S, Honda K, Uchimaru T, Mikami M, Tanabe K. The magnitude of the CH/π interaction between benzene and some model hydrocarbons. J Am Chem Soc 2000; 122:3746-53; http://dx.doi.org/10.1021/ja993972j.
54. Shanthi V, Ramanathan K, Sethumadhavan R. Exploring the role of C-H....pi interactions on the structural stability of single chain "all-alpha" proteins. Appl Biochem Biotechnol 2010; 160:1473-83; PMID:19266317; http://dx.doi.org/10.1007/s12010-009-8584-1.
55. Shapovalov G, Bass R, Rees DC, Lester HA. Open-state disulfide crosslinking between Mycobacterium tuberculosis mechanosensitive channel subunits. Biophys J 2003; 84:2357-65; PMID:12668444; http://dx.doi.org/10.1016/S0006-3495(03)75041-3.
56. Iscla I, Levin G, Wray R, Blount P. Disulfide trapping the mechanosensitive channel MscL into a gating-transition state. Biophys J 2007; 92:1224-32; PMID:17114217; http://dx.doi.org/10.1529/biophysj.106.090316.
57. Anishkin A, Akitake B, Kamaraju K, Chiang CS, Sukharev S. Hydration properties of mechanosensitive channel pores define the energetics of gating. J Phys Condens Matter 2010; 22:454120-31; PMID:21339607; http://dx.doi.org/10.1088/0953-8984/22/45/454120.